In Situ Intracellular Spectroscopy with Surface Enhanced Raman Spectroscopy (SERS)-Enabled Nanopipettes

Elina A. Vitol,[†] Zulfiya Orynbayeva,[‡] Michael J. Bouchard,[‡] Jane Azizkhan-Clifford,[‡] Gary Friedman,[†,*] and Yury Gogotsi[§,*]

[†]Department of Electrical and Computer Engineering, College of Engineering, Drexel University, Philadelphia, Pennsylvania 19104, [‡]Department of Biochemistry and Molecular Biology, College of Medicine, Drexel University, Philadelphia, Pennsylvania 19102, and [§]Department of Materials Science and Engineering, College of Engineering, Drexel University, Philadelphia, Pennsylvania 19104

ABSTRACT We report on a new analytical approach to intracellular chemical sensing that utilizes a surface-enhanced Raman spectroscopy (SERS)-enabled nanopipette. The probe is comprised of a glass capillary with a 100—500 nm tip coated with gold nanoparticles. The fixed geometry of the gold nanoparticles allows us to overcome the limitations of the traditional approach for intracellular SERS using metal colloids. We demonstrate that the SERS-enabled nanopipettes can be used for *in situ* analysis of living cell function in real time. In addition, SERS functionality of these probes allows tracking of their localization in a cell. The developed probes can also be applied for highly sensitive chemical analysis of nanoliter volumes of chemicals in a variety of environmental and analytical applications.

KEYWORDS: Raman spectroscopy · SERS · cells · biosensors · nanoparticles · trace analysis · nanopipette · micropipette

Surface-enhanced Raman spectroscopy (SERS) is a promising technique for label-free detection and analysis inside cells.[1−7] The primary mechanism of Raman scattering enhancement is related to the plasmonic focusing of an electromagnetic field on metal nanostructures.[8−10] SERS-active nanostructures are required to satisfy certain conditions in order to provide a strong Raman signal. First of all, the roughness of the metal surface should be smaller that the wavelength of the excitation field. Second, the wavelength of the excitation laser should correspond to the plasmon resonance wavelength of the SERS substrate. The latter can be controlled by changing the size, shape, and material of the metallic structures.[11−14] Originally discovered on electrochemically roughened surfaces, SERS is currently conducted using many other substrates such as metal nanoparticles of various shapes (spherical, triangular, prismatic),[1] nanoshells with a dielectric core and metal outer surface,[15] and highly ordered metal islands fabricated by lithographic techniques.[16]

SERS inside biological cells has been realized by introducing gold or silver nanoparticles through endocytosis. This technique was successfully applied for imaging DNA in single cells along with *in situ* studies of individual endosomes formed around a gold nanoparticle taken up by a cell.[4,17−20] However, uncontrollable aggregation of nanoparticles in cells poses difficulties because SERS signals are known to be highly sensitive to exact nanoparticle configuration.[8,13] Targeting of these nanoparticles to a specific location within cells through their functionalization[21] will also interfere with SERS analysis. An alternative solution to this problem would be to use the SERS substrates with fixed nanoparticle geometry.

Here we present the first SERS-active nanopipette for *in situ* intracellular analysis. This nanopipette is based on traditional glass pipettes widely employed in biology today. As a result, any standard equipment for cell microinjection, such as micromanipulators or fluid injectors can be used for cell analysis with SERS-active nanopipette. SERS functionality is added by incorporating gold nanoparticles on the outer surface pipette tip. We demonstrate that this allows us to track the location of the tip within the cell. For example, we show that the SERS spectra obtained with the nanopipette from within the nucleus are clearly different from those obtained within the cytoplasm and contain typical features associated with DNA. It is important to note that the tip of the nanopipette remains open after the functionalization with gold nanoparticles. Therefore, the SERS-active nanopipette can be used for concurrent drug injection and monitoring of cell response. Prior to combining these two functions, it is necessary to experimentally dem-

*Address correspondence to gogotsi@drexel.edu, gary@coe.drexel.edu.

Received for review August 24, 2009 and accepted October 26, 2009.

Published online November 5, 2009. 10.1021/nn9010768 CCC: $40.75

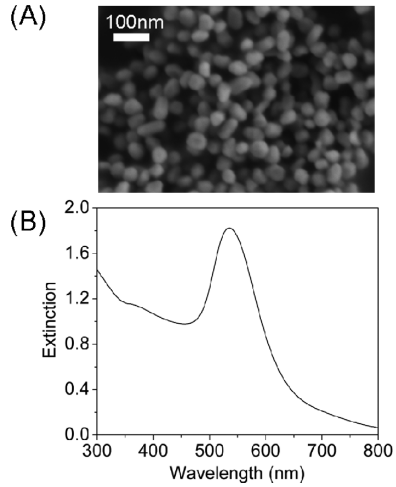

Figure 1. (A) Scanning electron micrograph (SEM) of the gold colloid used for fabricating the SERS-active nanopipette and (B) its extinction spectrum.

onstrate that the nanopipette has the necessary sensitivity to detect the changes in intracellular environment. This demonstration is the subject of the present work.

In this paper, we first discuss the design of the SERS-active nanopipette. In the next section, the chemical sensitivity of the nanopipette is accessed by measuring the characteristic SERS spectra from the tip of the nanopipette inserted in cell nucleus and cytoplasm. Special consideration is given to the effects of the nanopipette insertion on the cell. Finally, we demonstrate that the SERS-active nanopipette can be utilized for intracellular monitoring of living cell function in real time. Cell activity was stimulated by adding aqueous solution of KCl to the cell medium and the cell response was characterized by collecting SERS spectra from the nanopipette tip inserted in the cell cytoplasm.

RESULTS AND DISCUSSION

Optimization of the Nanoparticle Configuration for Nanopipette Design. It has been previously shown that 1 μm prismatic gold particles provide good SERS enhancement.[22] However, they are too large for intracellular applications and may cause fatal cell damage. In this work, equiaxial polygonal (close to spherical shape) gold nanoparticles were used. The average size of the nanoparticles (54 nm) was chosen as a result of the trade-off between the SERS sensitivity, which usually requires the nanoparticles to be in 30−100 nm range,[13] and the final size of the probe, which should be small enough to minimize potential effects on the cell during the probe insertion.[23] Scanning electron micrograph of these gold nanoparticles is shown in Figure 1A, along with the corresponding UV−vis absorption spectrum, Figure 1B. The diameter of the nanoparticles was measured using both SEM images and Zetasizer data.

Prior to fabricating the SERS nanopipette, the relationship between the surface density of gold nanoparticles on a glass substrate and the corresponding SERS enhancement was studied. A model system was constructed using planar glass slides coated with gold nanoparticles. SEM images of these substrates with different nanoparticle surface densities are shown in Figure 2A. UV−vis absorption spectra of all four substrates are similar to that of the nanoparticle colloid with the maximum absorption at about 540 nm (see Supporting Information, Figure S1). The corresponding SERS spectra, collected with 633 and 785 nm excitation lasers, are demonstrated in Figure 2B. At the lowest nanoparticle density (a), no SERS spectra were detected at either wavelength. Decreasing interparticle distance results in the appearance of the SERS spectra (b, c). Interestingly, at the highest particle density, the SERS signal obtained with 633 nm excitation laser becomes weaker as concluded from the increased spectral noise (spectrum d). In contrast, when the 785 nm laser is used to excite SERS of the same sample, the intensity of the SERS signal becomes significantly higher (spectrum d). This can be explained by the presence of the clustered gold nanoparticles which causes the red shift of the plasmon resonance, responsible for electromagnetic

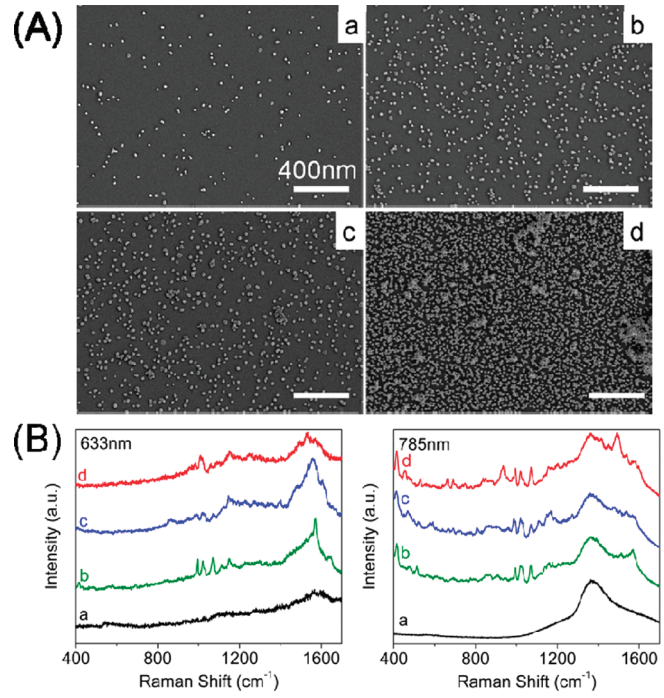

Figure 2. (A) SEM micrographs of the planar glass substrates coated with gold nanoparticles. The density of the attached nanoparticles is proportional to the time the glass substrates were immersed in the gold colloid. Samples shown in panels A,a−d correspond to 30 min, 2 h, 4 h, and 5 h of immersion, respectively. (B) SERS spectra of poly-L-lysine on gold-coated planar substrates with different surface density of the nanoparticles collected with 633 and 785 nm excitation laser. The graphs a−d correspond to the samples shown in panels A,a−d.

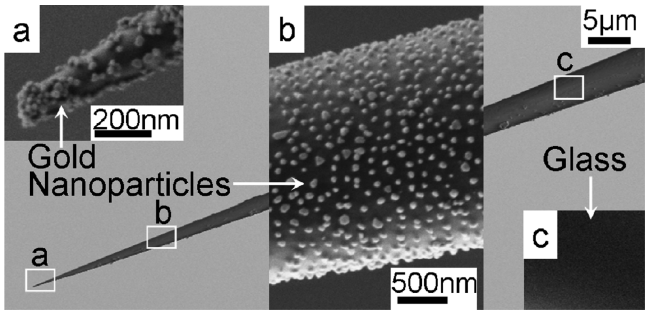

Figure 3. Scanning electron micrographs (SEM) of the SERS-active nanopipette. (a) The nanopipette tip covered with gold nanoparticles; (b) magnified view of the nanoparticles coverage of the nanopipette about 10 μm away from the tip; (c) bare glass surface of the nanopipette.

SERS enhancement.[13,14,24,25] Therefore, the 633 nm laser is not sufficient for exciting the plasmon resonance at the given nanoparticle density and size. The results suggest that the average distance between the nanoparticles has to be smaller than their diameter in order to achieve good SERS enhancement with a 633 nm excitation laser. When the surface density of the nanoparticles becomes very high and they form clusters, the plasmon resonance shifts to the longer wavelengths. In this case, SERS enhancement is higher with the 785 nm excitation laser.

SERS performance of the model planar substrates was tested on intact HeLa human cervical carcinoma cells. In addition, SERS signatures of isolated HeLa cell nuclei and mitochondria were collected on the model substrates with 40% nanoparticle surface density in order to confirm their specificity for cell studies (see Supporting Information, Figure S2). The protocols for organelle isolation and purification are described in Supporting Information. According to the collected data, the SERS fingerprint of the isolated HeLa nuclei is clearly different from that of the cell mitochondria or the cell membrane. Therefore, the selected nanoparticle configuration (shape and interparticle distance) ensures the desired specificity for intracellular SERS analysis.

SERS-Active Nanopipette. After establishing the optimal interparticle distance, the SERS-active nanopipette was fabricated. The nanopipette comprises a hollow glass capillary with a ~100 to 500 nm tip and is coated with gold nanoparticles. The overall length of the capillary is on the order of 10 cm and the outer diameter is 1 mm. Glass pipettes with such dimensions can be fitted into a standard micromanipulator and fluid injector, which are used for cell microinjection. Therefore, the SERS-active nanopipette does not require any specialized equipment and essentially represents a glass pipette, which is familiar to any cell biologist, supplemented with SERS functionality. In the future, this will ensure a smooth transition from the development model to the real world tool.

Figure 3 shows the scanning electron micrograph (SEM) of the SERS-active nanopipette. As shown in Figure 3a,b, the coverage of the gold nanoparticles is uniform. It is critical to emphasize that the nanoparticles are fixed on the nanopipette tip and the interparticle distance can be controlled by the nanopipette assembly conditions. The surface density of gold nanoparticles determines the characteristics of the SERS-activity of the nanopipette, according to the results presented in the previous section.

The nanopipette fabrication is discussed in detail in the Methods section. Briefly, the glass pipettes are prepared from commercial microcapillaries by laser pulling, then coated with poly-L-lysine polymer layer which contains positive NH_2 functional groups. At the last step, the nanopipettes are coated with negatively charged gold nanoparticles, which bind to the polymer from the colloid through the electrostatic interaction. The interaction time between the nanoparticles and the pipette, surface along with the nanoparticles colloid concentration are the major parameters controlling the nanoparticle surface density.

In principle, this functionalization technique can be applied to other substrates, for example, optical fibers. However such probes do not allow fluid injection and would require specialized equipment for inserting the probe into a cell. Carbon nanopipettes described in ref 23 can also be transformed into SERS probes.

Effect of the Nanopipette Insertion on Cell Integrity. We analyzed the effect of the SERS-active nanopipette insertion on the cytoskeleton network configuration in a living HeLa cell. An EYFP-fused β-actin expression construction was transfected into HeLa cells, and the produced fusion fluorescent protein was incorporated into the cytoskeleton. The confocal fluorescent image of the intact HeLa cell cytoskeleton is shown in Figure 4a. Insertion of the SERS-active nanopipette causes only

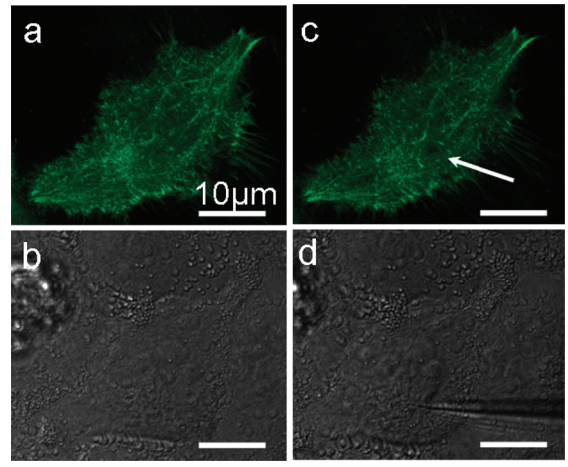

Figure 4. Confocal fluorescent images of the live HeLa cell cytoskeleton actin filaments before (a) and after (c) insertion of the SERS-active nanopipette. The corresponding differential contrast images are shown in panels b and d, respectively. The arrow shows the place of the probe's entrance in the cell.

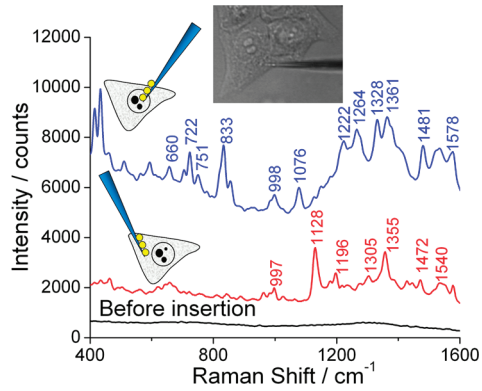

Figure 5. SERS spectra from the cell nucleus (upper spectrum) and cytoplasm (middle spectrum) obtained with the SERS-active nanopipette show distinctly different features. The bottom spectrum (black line) was collected from the nanopipette tip before insertion; 785 nm excitation laser was used. The spectra are offset for clarity.

a localized perforation of the actin network without damaging the rest of the cytoskeleton (Figure 4b). As a result, the probe insertion should not have a significant effect on the cell. Moreover, SEM analysis showed that the nanoparticles are strongly attached to the glass surface, so none of the particles peel off and remain inside a cell during the nanopipette insertion and after its removal from a cell. Microscopic analysis showed that the cells remain viable after the nanopipette withdrawal.

Navigating in Living Cells Using SERS-Active Nanopipette. The ability of the nanoprobe to provide a SERS signal from a specific location inside a cell was tested on adherent HeLa cells. A SERS-active nanopipette was inserted into a cell following a standard procedure used in cell biology for interrogating adherent cell cultures with glass pipettes. The nanopipette was fixed inside the pipette holder of the Eppendorf InjectMan NI2 micromanipulator. This micromanipulator allows precise control over the nanopipette movement. The stepper motor resolution is approximately 40 nm per step, according to the manufacturer. The nanopipette was positioned above a Petri dish with adherent HeLa cell culture and then directed toward the cells at a 45° angle. This was continuously monitored under the Raman microscope with a 50× long working distance objective. Detailed requirements for minimally damaging pipette insertion can be found elsewhere.[26] During the data acquisition, the excitation laser was always focused on the nanopipette tip.

The SERS spectrum collected from the nanopipette tip inserted in the cell nucleus, whose outlines could be observed through regular bright field microscopy, is clearly different from that collected inside the cell cytoplasm (Figure 5). The data presented in Figure 5 represents the averages of at least five different experiments, conducted on multiple cells with SERS-active nanopipettes. It is important to note that the SERS spectra measured from the same location inside a cell demonstrate certain variability in terms of the intensity (10−15%) and, to a minor extent, in the location of spectral peaks. The latter can vary by 10−20 cm^{-1}, which is within the expected range normally observed in SERS.

The nuclear spectrum has features that are primarily attributable to its high protein and amino acid content (1076, 1222, 1264, 1328, 1361 cm^{-1}), and to DNA (660, 722 cm^{-1}).[4,27] The cytoplasmic SERS spectrum does not show the DNA bands. However, it still contains the peaks related to the protein constituents of the cytoplasm (1128, 1540, 1355 cm^{-1}). At the same time, the 1196 cm^{-1} peak is most likely associated with the phenylalanine. As expected, the cytoplasmic phenylalanine signal is stronger than that of the nucleus.[17,28] It is important to stress again that nanopipette insertion does not cause fatal damage to a cell.

Data Reproducibility. Irregularities of the SERS substrates are considered to be the major reason for the poor reproducibility of SERS spectra apart from spectral blinking.[29] The irreproducibility problem can be solved by creating SERS substrates with highly uniform metal nanostructures. One of the examples is the nanosphere lithography technique which has been successfully applied for creating SERS active substrates and obtaining highly reproducible spectra of various materials.[30] However, in the case of biological and especially cellular SERS studies, special consideration has to be given to the problem of spectral reproducibility. On one hand, it is important to have a SERS substrate with a uniform configuration of metal nanostructures. This was the major motivation for creating the SERS-active nanopipette with nanoparticles fixed on the surface as opposed to using a nanoparticle colloid which tends to aggregate inside the cell in a way that is difficult to control. On the other hand, it is critical to understand that a highly sensitive SERS sensor that allows detection of compositional changes in the intracellular environment with a submicrometer resolution will inevitably provide different SERS spectra from different locations inside a cell due to the cell heterogeneity. However, the difference between the spectra should still be within the same range if the same cell compartment is being analyzed.

To test the performance of the SERS-active nanopipette, we compare the data obtained with the SERS-active nanopipette from a pure chemical (poly-L-lysine) and the heterogeneous HeLa cell cytoplasm. The spectra were collected from multiple cells. The results are presented in the principal components space in Figure 6. Principal component analysis is a multivariate data analysis technique that is widely used in spectroscopy for facilitating data interpretation by reducing its dimensionality and calculating the degree of correlation (similarity) between the spectra[31] (see Methods for details). The data presented in Figure 6 shows the original SERS spectra mapped into the new coordinate system

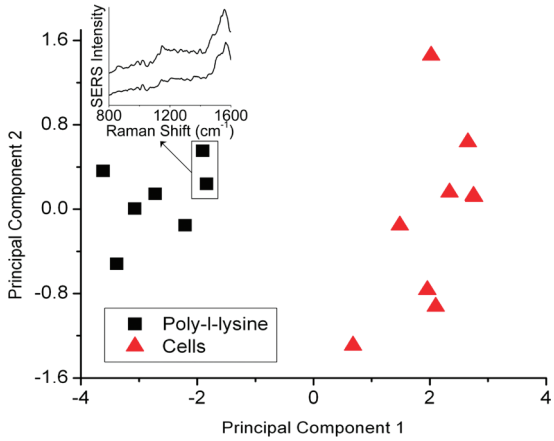

Figure 6. Principal component analysis of the data obtained with SERS-active nanopipette with poly-L-lysine (squares) and HeLa cells (triangles). Each point in the principal component space represents a SERS spectrum. The data was collected with the 633 nm excitation laser. The distance between the data points is related to the degree of similarity between two SERS spectra. To provide a reference, the inset graph shows the SERS spectra corresponding to two data points in the principal component space.

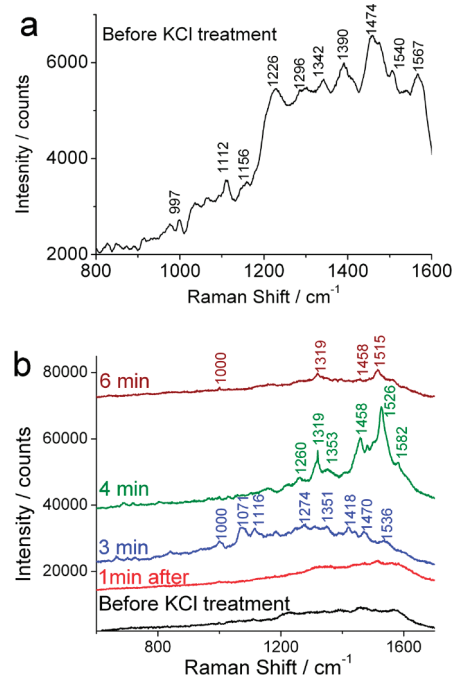

Figure 7. SERS spectrum collected from the nanopipette tip inserted in the HeLa cell cytoplasm (a) and representative time-resolved spectra showing HeLa cell response to treatment with KCl aqueous solution with the SERS-active nanopipette (b). Time-dependent variation of the cytoplasmic signal has been observed. Data acquisition time was 20 s, a 633 nm excitation laser was used. The spectra in panel b are offset for clarity.

defined by the principal components. Here the principal components represent a coordinate system rather than a projection of the original data on the new axes. The results of the data analysis demonstrate that the data scatter for a pure chemical is significantly lower (small variation of both components) than that for the cell cytoplasm (small variation of component 1, but a larger variation of component 2). At the same time, the spectra from the HeLa cell cytoplasm are still located within the range, as expected. Therefore, the SERS nanopipette provides the well reproducible data. It is highly important, however, to take the effect of the cell interior heterogeneity into account. New methods, such as the recently introduced thermal relaxation for DNA, will likely further improve the specificity of *in situ* analysis using SERS-active nanopipettes.[3] In addition, according to the results obtained in multiple experiments, repeatability of the data obtained with different nanopipettes is within the range observed for different cells. Therefore, the slight variation in the interparticle distance for different probes does not cause a significant signal variation.

Intracellular Sensing with SERS-Active Nanopipette. The possibility of monitoring cell activity by SERS-active nanopipettes upon the application of the external stimulus was studied in this work. Previously, SERS has been applied for monitoring the uptake of dilute solution of doxorubicin (antitumor drug) by a living cancer cell.[20] However, to the best of our knowledge, the actual physiological cellular response to a pharmaceutical compound or any external stimulus application has never been assessed using *in situ* SERS. In this work, we performed the assessment of the real time cell response to the treatment with aqueous solution of KCl.

The nanopipette was inserted into the cytoplasmic region of a living adherent cell, and the background spectrum was collected (Figure 7a). After that, an aqueous KCl solution was added to the cell medium to achieve a final concentration of 55 mM. Time sequence of the SERS spectra from the cell interior was collected (Figure 7b). It is important to emphasize that KCl was used to trigger cell activity by providing the external cell stimulus. The configuration of the gold nanoparticles was not affected by KCl since the nanoparticles were fixed on the nanopipette surface. Treated cells exhibited almost a 5-fold increase in the Raman scattering intensity, compared to the Raman spectra obtained on untreated cells, as can be seen from comparing Figure 7 panels a and b. The maximum intensity amplitude of SERS spectra before and after KCl treatment was about 4000 and 20000 CCD counts, respectively (Figure 7b). Because of this, the SERS spectrum collected from the nanopipette tip inserted in the HeLa cell cytoplasmic region appears almost featureless compared to the spectra collected after the treatment with KCl solution (Figure 7b), when plotted without intensity normalization.

From a biological point of view, increased levels of extracellular potassium ions cause depolarization of the cell membrane potential due to the decrease in the equilibrium potential for this ion.[32] The loss of cytosolic water, resulting from an increase in environmental

osmolarity and plasma membrane depolarization, can lead to alterations in the cytosolic concentration of cellular colloids, such as proteins and organic phosphates, and the hydration level of proteins.[33,34] The hydration state of cellular components and the resulting conformational modifications of proteins are the likely cause of the observed SERS signal modulation. This is indicated by the appearance of high intensity peaks in the 1200−1500 cm^{-1} region (Figure 7). It is important to note that the intensities of certain spectral peaks exhibited a dynamic behavior after the KCl treatment. The reason for the appearance of 1319, 1260, 1515, and 1526 cm^{-1} SERS peaks at different time points can be associated with the induced expression of various types of stress proteins.[35] The change in environmental osmolarity triggers the cellular adaptive mechanism, which leads not only to the induction but also to the suppression of specific proteins. This process occurs primarily in the first several minutes after the addition of KCl to the cell medium. The dynamics of this complex mechanism manifests itself in the recorded SERS spectra. Alterations of the peak profile at different time points reflect dynamic cellular processes in response to perturbations of extracellular environment. After 6 min, the cell volume regulatory mechanism restores the initial iso-osmotic state of the cell. This is reflected in the SERS spectrum, which becomes again similar to that collected before the cell treatment with KCl.

These results demonstrate that the SERS-active nanopipette works as a real time sensor of local intracellular biochemical processes. It is critical to emphasize that this experiment was performed without adding any labels to the cell and the cell activity was monitored *in situ*. The level of chemical sensitivity offered by SERS is superior to that of any other currently available biological techniques. These results can be further extended to combining the basic nanopipette fluid delivery function with the SERS sensing. By carefully controlling the injection pressure and time, it should be possible to deliver femtoliters of fluid into a cell and simultaneously assess the cell response in real time; a recently introduced technique which uses "electrostatic driving force" for navigating specific molecules to the SERS substrate could further improve the performance of the SERS-active nanopipette.[36] Combination of this method with the nanopipette would allow one to selectively target different molecules in living cells with a higher level of selectivity. Finally, applications of a SERS-active nanopipette are not limited to cellular studies, and the nanopipette also enables highly localized chemical analysis of low concentration chemicals, which is of a great importance for microanalytical chemistry, environmental, and forensic studies.

CONCLUSIONS

In summary, a SERS-active nanopipette for *in situ* intracellular observations has been developed. We have demonstrated that the positioning of the nanopipette tip, either within the cell nucleus or cytoplasm, can be clearly distinguished through the measured SERS. Feedback on the positioning of the nanopipette tip within cells will provide valuable information during cell injections, single cell surgery or for *in situ* study of cell signaling. Good reproducibility of the cellular SERS signal was obtained, suggesting that, with some optimization, it should be possible to determine the proximity of the tip to specific cell organelles and to measure the concentration of various molecular species. For the first time, *in situ* cell response to the changes in its environment was measured by using an intracellular SERS probe.

METHODS

Synthesis of Gold Nanoparticles. Gold colloid was synthesized using the Turkevitch method.[37] The protocol was modified to optimize the size of the gold nanoparticles. Hydrogen tetrachloroaurate ($HAuCl_4$) aqueous solution (10 mL, 2.5 mM concentration) was boiled and then 2 mL of sodium citrate was added with vigorous agitation. The mixture was stirred until it became deep red in color, and then removed from the heat. After cooling down, the colloid was left to reach equilibrium in the dark for 1 week. This protocol yielded gold nanoparticles with the average diameter of 54 nm as confirmed by scanning electron microscopy analysis. Zeta potential, related to the surface charge of the nanoparticles, was measured to be approximately −40 mV.

Fabrication of the SERS-Active Nanopipettes. Glass nanopipettes were prepared by pulling a hollow borosilicate glass capillary to a 150 nm tip diameter. The characteristics of the glass capillary are as follows: length of 10 mm, inner diameter of 0.75 mm, and outer diameter of 1 mm. The glass capillaries were purchased from Sutter Instrument (BF100-78-10). The dimensions of the resulting nanopipette were determined by the parameters on the micropipette puller (Laser based micropipette puller P-2000, Sutter Instrument, USA). After pulling, the glass pipettes were soaked in a mixture of 95% ethanol and 1 M aqueous solution of sodium hydroxide for 1 h. After washing with 15 MΩ deionized water, the pipettes were left to dry at room temperature. The pipettes were then dip-coated with the 0.001 wt % aqueous solution of poly-L-lysine. Polymer coating enabled the immobilization of gold nanoparticles on the glass due to the electrostatic interaction between the positively charged terminal NH_2 groups of the poly-L-lysine and the negatively charged Au nanoparticles.[38]

Characterization Techniques. Raman spectroscopy analysis was performed using a micro-Raman spectrometer (Renishaw, RM 1000/2000) equipped with a 632.8 nm HeNe laser (1800 lines/mm grating) and a diode laser operating at 785 nm wavelength (1200 lines/mm grating). The laser source was focused on the sample through a long working distance 50× objective to a spot size of approximately 2 μm. The acquisition time for all spectra was 10−20 s. Data analysis was performed using the Renishaw Wire 2.0 software. SEM images were collected with the field emission scanning electron microscope Zeiss Supra 50 VP. Before imaging, the gold-functionalized glass slides were sputter-coated with 2 nm of Pt/Pd. The images were collected at 5 kV accelerating voltage. SEM images of the SERS-active nanopipette were acquired at 0.7−2 kV accelerating voltage without any conductive coating. UV−vis absorption spectra were acquired using a UV−vis spectrophotometer (Thermo Scientific, Evolution 600).

The zeta potential of gold nanoparticles was measured using a Zetaziser Nano ZS (Malvern Instruments, UK). Confocal fluorescence microscopy was carried out using the Olympus FluoView 1000 microscope, comprising an Olympus IX 81 inverted microscope equipped with a laser scanning confocal system.

Data Analysis. Principal component analysis (PCA) is a method of analyzing complex sets of data with multiple variables. The technique facilitates identification of hidden relationships between data sets by reducing their dimensionality and representing the data in the new coordinate system. Raman spectrum can be considered as a data matrix where the first column represents the Raman shift and the second column contains the corresponding signal intensity. For PCA of n spectra with p data points, an n-by-p matrix is constructed, where each row represents a Raman intensity spectrum. The purpose of the PCA is to find a new p-dimensional orthogonal coordinate system where the data projection on each coordinate axis has a sequentially maximal variance.[39] Each projection corresponds to a linear combination of the original data, with the first projection having the maximum variance and representing the first principal component. Here, PCA was performed using Matlab calculation environment.

Acknowledgment. This work was supported by a W. M. Keck Foundation grant to establish the Keck Institute for Attofluidic Nanotube-Based Probes at Drexel University and by the Pennsylvania Nanotechnology Institute (NTI) through Ben Franklin Technology Partners of Southeastern Pennsylvania. Scanning electron microscopy and Raman spectroscopy analyses were conducted at the Centralized Research Facilities at Drexel University.

Supporting Information Available: UV−vis absorption spectra of model SERS substrates, SERS spectra of different cell organelles, and supplementary cell culture protocols. This material is available free of charge *via* the Internet at http://pubs.acs.org.

REFERENCES AND NOTES

1. Nie, S.; Emory, S. R. Probing Single Molecules and Single Nanoparticles by Surface-Enhanced Raman Scattering. *Science* **1997**, *275*, 1102.
2. Cao, Y. C.; Jin, R.; Mirkin, C. A. Nanoparticles with Raman Spectroscopic Fingerprints for DNA and RNA Detection. *Science* **2002**, *297*, 1536.
3. Barhoumi, A.; Zhang, D.; Tam, F.; Halas, N. J. Surface-Enhanced Raman Spectroscopy of DNA. *J. Am. Chem. Soc.* **2008**, *130*, 5523.
4. Kneipp, J.; Kneipp, H.; McLaughlin, M.; Brown, D.; Kneipp, K. *In Vivo* Molecular Probing of Cellular Compartments with Gold Nanoparticles and Nanoaggregates. *Nano Lett.* **2006**, *6*, 2225.
5. Kneipp, K.; Wang, Y.; Kneipp, H.; Perelman, L. T.; Itzkan, I.; Dasari, R.; Feld, M. S. Single Molecule Detection Using Surface-Enhanced Raman Scattering (SERS). *Phys. Rev. Lett.* **1997**, *78*, 1667.
6. McFarland, A. D.; Young, M. A.; Dieringer, J. A.; Van Duyne, R. P. Wavelength-Scanned Surface-Enhanced Raman Excitation Spectroscopy. *J. Phys. Chem. B* **2005**, *109*, 11279.
7. Isola, N. R.; Stokes, D. L.; Vo-Dinh, T. Surface Enhanced Raman Gene Probe for HIV Detection. *Anal. Chem.* **1998**, *70*, 1352.
8. Schatz, G. C. Using Theory and Computation to Model Nanoscale Properties. *Proc. Natl. Acad. Sci. U.S.A.* **2007**, *104*, 6885.
9. Moskovits, M. Surface-Enhanced Spectroscopy. *Rev. Mod. Phys.* **1985**, *57*, 783.
10. Wang, H.; Kundu, J.; Halas, N. J. Plasmonic Nanoshell Arrays Combine Surface-Enhanced Vibrational Spectroscopies on a Single Substrate. *Angew. Chem., Int. Ed.* **2007**, *46*, 9040.
11. Oldenburg, S. J.; Averitt, R. D.; Westcott, S. L.; Halas, N. J. Nanoengineering of Optical Resonances. *Chem. Phys. Lett.* **1998**, *288*, 243.
12. Khoury, C. G.; Norton, S. J.; Vo-Dinh, T. Plasmonics of 3-D Nanoshell Dimers Using Multipole Expansion and Finite Element Method. *ACS Nano* **2009**, *3*, 2776–2788.
13. Moskovits, M. Surface-Enhanced Raman Spectroscopy: A Brief Retrospective. *J. Raman Spectrosc.* **2005**, *36*, 485.
14. Talley, C. E.; Jackson, J. B.; Oubre, C.; Grady, N. K.; Hollars, C. W.; Lane, S. M.; Huser, T. R.; Nordlander, P.; Halas, N. J. Surface-Enhanced Raman Scattering from Individual Au Nanoparticles and Nanoparticle Dimer Substrates. *Nano Lett.* **2005**, *5*, 1569.
15. Jackson, J. B.; Halas, N. J. Silver Nanoshells: Variations in Morphologies and Optical Properties. *J. Phys. Chem. B* **2001**, *105*, 2743.
16. Hulteen, J. C.; Vanduyne, R. P. Nanosphere Lithography—A Materials General Fabrication Process for Periodic Particle Array Surfaces. *J. Vac. Sci. Technol., A* **1995**, *13*, 1553.
17. Kneipp, K.; Haka, A. S.; Kneipp, H.; Badizadegan, K.; Yoshizawa, N.; Boone, C.; Shafer-Peltier, K. E.; Motz, J. T.; Dasari, R. R.; Feld, M. S. Surface-Enhanced Raman Spectroscopy in Single Living Cells Using Gold Nanoparticles. *Appl. Spectrosc.* **2002**, *56*, 150.
18. Kneipp, J. In *Surface-Enhanced Raman Scattering: Physics and Applications*; Kneipp, K., Moskovits, M., Kneipp, H., Eds.; Springer-Verlag: Berlin, 2006; Vol. 103, p 335.
19. Graham, D.; Mallinder, B. J.; Smith, W. E. Surface-Enhanced Resonance Raman Scattering as a Novel Method of DNA Discrimination. *Angew. Chem., Int. Ed.* **2000**, *39*, 1061.
20. Nabiev, I. R.; Morjani, H.; Manfait, M. Selective Analysis of Antitumor Drug-Interaction with Living Cancer Cell as Probed by Surface-Enhanced Raman Spectroscopy. *Eur. Biophys. J.* **1991**, *19*, 311.
21. Kickhoefer, V. A.; Han, M.; Raval-Fernandes, S.; Poderycki, M. J.; Moniz, R. J.; Vaccari, D.; Silvestry, M.; Stewart, P. L.; Kelly, K. A.; Rome, L. H. Targeting Vault Nanoparticles to Specific Cell Surface Receptors. *ACS Nano* **2008**, *3*, 27.
22. Sabur, A.; Havel, M.; Gogotsi, Y. SERS Intensity Optimization by Controlling the Size and Shape of Faceted Gold Nanoparticles. *J. Raman Spectrosc.* **2008**, *39*, 61.
23. Schrlau, M. G.; Dun, N. J.; Bau, H. H. Cell Electrophysiology with Carbon Nanopipettes. *ACS Nano* **2009**, *3*, 563.
24. Hao, E.; Schatz, G. C. Electromagnetic Fields around Silver Nanoparticles. *J. Chem. Phys.* **2004**, *120*, 357.
25. Reinhard, B. M.; Siu, M.; Agarwal, H.; Alivisatos, P.; Liphardt, J. Calibration of Dynamic Molecular Rule Based on Plasmon Coupling between Gold Nanoparticles. *Nano Lett.* **2005**, *5*, 2246.
26. Lappe-Siefke, C.; Maas, C.; Kneussel, M. Microinjection into Cultured Hippocampal Neurons: A Straightforward Approach for Controlled Cellular Delivery of Nucleic Acids, Peptides, and Antibodies. *J. Neurosci. Methods* **2008**, *175*, 88.
27. Zeiri, L.; Bronk, B. V.; Shabtai, Y.; Eichler, J.; Efrima, S. Surface-Enhanced Raman Spectroscopy as a Tool for Probing Specific Biochemical Components in Bacteria. *Appl. Spectrosc.* **2004**, *58*, 33.
28. Puppels, G. J.; Demul, F. F. M.; Otto, C.; Greve, J.; Robertnicoud, M.; Arndtjovin, D. J.; Jovin, T. M. Studying Single Living Cells and Chromosomes by Confocal Raman Microspectroscopy. *Nature* **1990**, *347*, 301.
29. Dong, L. Q.; Zhou, J. Z.; Wu, L. L.; Dong, P.; Lin, Z. H. SERS Studies of Self-Assembled DNA Monolayer—Characterization of Adsorption Orientation of Oligonucleotide Probes and Their Hybridized Helices on Gold Substrate. *Chem. Phys. Lett.* **2002**, *354*, 458.
30. Haynes, C. L.; Van Duyne, R. P. Plasmon-Sampled Surface-Enhanced Raman Excitation Spectroscopy. *J. Phys. Chem. B* **2003**, *107*, 7426.
31. Mahadevan-Jansen, A.; Mitchell, M. F.; Ramanujam, N.; Malpica, A.; Thomsen, S.; Utzinger, U.; Richards-Kortum, R. Near-Infrared Raman Spectroscopy for *in Vitro* Detection of Cervical Precancers Photochem. *Photobiol.* **1998**, *68*, 123.

32. Doyle, D. A.; Cabral, J. M.; Pfuetzner, R. A.; Kuo, A. L.; Gulbis, J. M.; Cohen, S. L.; Chait, B. T.; MacKinnon, R. The Structure of the Potassium Channel: Molecular Basis of K^+ Conduction and Selectivity. *Science* **1998**, *280*, 69.
33. Jennings, M. L.; Schulz, R. K. Swelling-Activated KCl Cotransport in Rabbit Red Cells: Flux Is Determined Mainly by Cell Volume Rather Than Shape. *Am. J. Physiol.-Cell Physiol.* **1990**, *259*, C960.
34. McCarty, N. A.; O'Neil, R. G. Calcium Signaling in Cell Volume Regulation. *Physiol. Rev.* **1992**, *72*, 1037.
35. Kregel, K. C. Heat Shock Proteins: Modifying Factors in Physiological Stress Responses and Acquired Thermotolerance. *J. Appl. Physiol.* **2002**, *92*, 2177.
36. Lacharmoise, P. D.; Le Ru, E. C.; Etchegoin, P. G. Guiding Molecules with Electrostatic Forces in Surface Enhanced Raman Spectroscopy. *ACS Nano* **2008**, *3*, 66.
37. Turkevitch, J.; Stevenson, P. C.; Hillier, J. Nucleation and Growth Process in the Synthesis of Colloidal Gold. *Discuss. Faraday Soc.* **1951**, *11*, 55.
38. Freeman, R. G.; Grabar, K. C.; Allison, K. J.; Bright, R. M.; Davis, J. A.; Guthrie, A. P.; Hommer, M. B.; Jackson, M. A.; Smith, P. C.; Walter, D. G.; Natan, M. J. Self-Assembled Metal Colloid Monolayers—An Approach to SERS Substrates. *Science* **1995**, *267*, 1629.
39. Green, P. E.; Carrol, J. D. *Analyzing Multivariate Data*; Dryden Press: Hinsdale, Il, 1978.